SolarPACES 2024, 30th International Conference on Concentrating Solar Power, Thermal, and Chemical Energy Systems

Thermal Energy Storage Materials, Media, and Systems

https://doi.org/10.52825/solarpaces.v3i.2339

© Authors. This work is licensed under a Creative Commons Attribution 4.0 International License

Published: 18 Nov. 2025

Performance Evaluation of Fluidized Bed Reactors for TCES Based on the CaO/CaCO₃ and MnAl₂O₄/MnAl₂O_{4-δ} Systems

Maria Anna Murmura^{1,*} , Valentina Biagioni¹, and Maria Cristina Annesini¹

¹Università di Roma "La Sapienza", Italy

*Correspondence: Maria Anna Murmura, mariaanna.murmura@uniroma1.it

Abstract. The following work presents an analysis of the fluidization conditions and performance of fluidized bed reactors (FBRs) working in the discharge phase for two different systems, namely CaO/CaCO₃ and MnAl₂O₄/MnAl₂O_{4- δ}. The two systems have been chosen for their different operating temperatures and fluidization properties, thereby allowing an evaluation of the feasibility of working with fluidized bed reactors under a range of operating conditions. The results show that, though the MnAl₂O₄/MnAl₂O_{4- δ} system is capable of achieving a higher efficiency, with about 90% of the heat released by the reaction being transferred to the gas, the total amount of energy released by the solid per unit mass is significantly lower (approx. 100 J/g) compared to the performance achieved by the CaO/CaCO₃ system (approx. 800 J/g). The results obtained for the carbonate system have been found to be in very good agreement with those reported in the literature based on a more complex and computationally challenging model.

Keywords: Fluidized Bed Reactors, Thermochemical Energy Storage, Calcium Looping, Spinel Oxidation

1. Introduction

Thermochemical energy storage (TCES) is based on the storage of chemical energy making use of reversible thermochemical reactions characterized by a high reaction enthalpy. Gassolid reacting systems may be roughly divided into three groups, depending on whether they are based on the carbonation/decarbonation of metal carbonates, reduction/oxidation of metal oxides, or hydration/dehydration of metal hydroxides. As for the reactor configurations, all the classical types of gas-solid reactors have been considered for TCES: fixed bed reactors are low cost, easy to design and operate, but reactors suffer from poor heat and mass transfer and require the use of large solid particles to limit pressure drops. Fluidized bed reactors (FBRs) can count on remarkably high heat transfer coefficients and efficient solid mixing, but the hydrodynamics are difficult to model and operate [1,2]. The main difficulty lies in the fact that the fluidization conditions depend on gas and solid densities, which in the case of gas-solid reactions may vary significantly in the course of the process, introducing complexities in both the design and control of the reaction and reducing operating flexibility. The aim of this work has been to carry out a preliminary investigation of the fluidization properties of two TCES systems, namely those based on the CaO/CaCO₃ and MnAl₂O₄/MnAl₂O_{4-δ} couples, based on reactions (1) and (2), respectively

$$CaCO3(s) = CaO(s) + CO2(g) \quad \Delta H = 178 \, kJ/mol \tag{1}$$

$$MnAl_2O_{4(s)} = MnAl_2O_{4-\delta(s)} + \frac{\delta}{2}O_{2(g)} \quad \Delta H = 22.4 \, kJ/mol$$
 (2)

These two reactive systems have been chosen because of their different operating temperatures, ranging between 700 and 900°C for the calcium carbonate system and between 500 and 650°C for the manganese aluminum spinel system, respectively. The other significant difference between the two systems consists in the fact that the former is characterized by a noticeable change in the solid density in the course of the reaction, due to the sizeably different molar mass of calcium carbonate compared to calcium oxide, while the latter is characterized by virtually constant solid density because of the small value of the stoichiometric coefficient, δ , which usually varies between 0.02 and 0.04 [3]. More details regarding these two reactive systems may be found in the literature (see, e.g. [3,4]). In this work, the value of δ in reactions(2) has been set to 0.04. The analysis presented here therefore allows to assess the feasibility of working with fixed bed reactors under a wide range of conditions.

2. Study of Fluidization Conditions

The minimum fluidization velocity may be evaluated starting by setting the equivalence between drag force and gravity, using the Ergun equation to evaluate pressure drops

$$\frac{g\rho_{\rm f}(\rho_s - \rho_{\rm f})d^3}{\mu^2} = 150 \frac{1 - \varepsilon_{mf}}{\varepsilon_{mf}^3} \frac{u_{mf}d\rho_f}{\mu} + \frac{1.75}{\varepsilon_{mf}^3} \left(\frac{u_{mf}d\rho_f}{\mu}\right)^2 \tag{3}$$

where u_{mf} is the minimum fluidization velocity, d is the particle diameter, μ is the fluid viscosity and ρ_f its density, and ε_{mf} is the bed void fraction under minimum fluidization conditions. Increasing the gas velocity may lead to a transition toward a bubbling bed regime, depending on particle type. Such characteristic velocity mainly depends on particle size and density, as well as gas density and viscosity [5]. The transition to fast fluidization, in which the solid could be entrained by the gas leaving the reactor takes place when the gas velocity is increased to its terminal value, u_t , which may be defined as

$$u_t = \left(\frac{4d_p(\rho_s - \rho_f)g}{3\rho_g C_D}\right)^{\frac{1}{2}} \tag{4}$$

where C_D is the drag coefficient, for which several empirical correlations have been developed, including the one proposed by Haider and Levenspiel [6]

$$C_D = \frac{24}{Re_p} + 3.3643Re_p^{0.3471} + \frac{0.4607Re_p}{Re_p + 2682.5} \quad ; \quad Re_p = \frac{d_p u_t \rho_f}{\mu}$$
 (5)

The characteristic velocities for the particles to be employed in the two reactive systems are reported in Tables 1 and 2. The particle diameter was set to 200 μm for the particles employed in the carbonate system, with a solid density of 1448 kg/m³ for CaO/Mayenite and 2512 kg/m³ for CaCO3/Mayenite and 150 μm for the spinel, with solid density of 780 kg/m³, based on information presented in the literature [3,4]. The bed void fraction under minimum fluidization conditions was set to 0.4 in both cases. The gas viscosity was considered to be independent of composition, given the very close values of the viscosities of CO₂ and air. Note that, in Table 2, the effects of solid conversion and gas composition were not considered because, given the low value of δ , the solid and gas densities remain virtually unchanged throughout the process.

Table 1. Minimum fluidization and terminal velocities for CaO/Mayenite and CaCO₃/Mayenite for different gas compositions at 873 K.

	CO ₂		50% CO₂/50% air		air	
	CaO/ mayenite	CaCO₃/ mayenite	CaO /mayenite	CaCO₃/ mayenite	CaO/ mayenite	CaCO3/ mayenite
u_{mf} [m/s]	0.043	0.074	0.043	0.074	0.043	0.074
u_t [m/s]	0.785	1.10	0.838	1.19	0.903	1.30

Table 2. Minimum fluidization and terminal velocities for MnAl₂O_{4-ō} at different temperatures for the charging and discharging phases in air.

	773 K	873 K	923 K	973 K	1023 K	1073 K
	discharge			charge		
u_{mf} [m/s]	0.013	0.013	0.013	0.013	0.013	0.013
u_t [m/s]	0.355	0.361	0.364	0.366	0.369	0.371

Given the high density of the solid, the minimum fluidization and terminal velocities are almost independent of the gas density, i.e. of temperature and gas composition; indicating that these materials allow for a flexible operation of the reactor under a wide range of operating conditions. For the CaO/CaCO₃ system, the gas flow rate should be chosen so as to work under adequate fluidization conditions regardless of the degree of conversion and, consequently, solid density. This should be feasible given the high ratio between terminal and minimum fluidization velocities.

3. Reactor Model Development

We start the description of the model development considering the CaO/CaCO₃ system and then move on to discuss the simplifying assumptions that can be introduced when extending it to the spinel system. For the former reactive couple, the model was developed under the assumptions of (i) plug flow of the gas, (ii) perfectly mixed solid, and (iii) reaction described by a multigrain, shrinking-core model considering the process to be kinetically limited by the surface reaction [4], and (iv) adiabatic reactor. It should be noted that, in this system, the solid has two characteristic dimensions: the size of the CaO/mayenite particles, which determines the fluidization properties, and the size of the CaO granules making up the particles and that affects the reaction kinetics. Here we consider all heat and mas transfer resistances within the particle to be negligible, in accordance with the results of preliminary analyses. Under these assumptions, the CaO conversion is given by

$$X_{CaO} = 1 - (1 - t/\tau)^3 \quad ; \quad \tau = \frac{c_{CaO}R_g^0}{k_s(c_{CO_2}^g - c_{CO_2}^{eq})}$$
 (6)

where $\mathcal{C}_{\mathcal{C}a\mathcal{O}}$ is the molar concentration of CaO in the granule (30714 mol/m³), R_g^0 is its initial radius of the CaO grains making up each CaO/Mayenite particle (1.37x10⁻⁷ m), and k_s is the temperature-independent kinetic constant, (3.75 × 10⁻⁶ m/s [1]). $c_{\mathcal{C}O_2}^g$ e $c_{\mathcal{C}O_2}^{eq}$ are the CO₂ concentrations in the gas and under equilibrium conditions, respectively. The overall and CO₂ mass balance equations are given by

$$\frac{(\partial c_{tot}(z)u(z))}{\partial z} = -N_{CO_2,g\to s}a_s^v \quad ; \quad \frac{(\partial c_{CO_2}(z)u(z))}{\partial z} = -N_{CO_2,g\to s}a_s^v \tag{7}$$

where $N_{CO_2,g\to s}$ is the CO₂ flux being transferred from the gas to the solid because of the reaction, and a_s^v is the solid surface area per reactor volume. These two values are given by

$$a_s^v = \frac{n_g 4\pi R_g^2}{V_r}$$
 ; $N_{CO_2,g\to s} = (1 - X_{CaO})^{2/3} k (\bar{c}_{CO_2} - c_{CO_2,eq})$; $n_g = \frac{0.75 M_s}{\frac{4}{3}\pi R_g^3 \rho_{CaO}}$ (8)

where n_g is the number of CaO granules in the reactor, where M_s is the solid mass, while \bar{c}_{CO_2} is the average CO₂ concentration in the gas. It is worth noting that, since the solid is perfectly mixed, it is exposed to a CO₂ concentration that is the average of its value along the length of the solid bed. The energy balance equations in the gas and solid are given by Eq. (9).

$$\rho_g c_{p,g} \frac{\partial T}{\partial t} + \frac{1}{A} F_{TOT} \bar{c}_p \frac{\partial T}{\partial z} = h a_s^v (T_s - \bar{T}) \quad ; \quad \rho_s c_{p,s} \frac{dT_s}{dt} = -h a_s^v (T_s - \bar{T}) - N_{CO_2,g \to s} a_s^v \Delta H_r$$
 (9)

where h is the heat transfer coefficient between gas and solid and is set to 300 W/m²K, ΔH_r is the heat of reaction, and \bar{T} and T_s are the average tempertures of the gas and the temperature of the solid, respectively. It is worth noting that, given the high heat transfer rate in fluidized bed reactors, even significant changes of h around the value estimated do not lead to appreciable differences in the model result. The effect of the gas flow rate on the height of the bed, H, was evaluated through Eq.(10)

$$\frac{\mathbf{u}_{\mathbf{g}}}{\mathbf{u}_{\mathbf{t}}} = \varepsilon^{\mathbf{n}} \tag{10}$$

with n equal to 6 [7]. Both the gas and terminal velocities change along the length of the reactor, meaning that the void fraction changes both in time and within the reactor. The height of the bed is therefore evaluated based on the average void fraction as

$$\bar{\varepsilon} = \frac{1}{H} \int_0^H \varepsilon dz$$
 ; $M_{solid} = HA\rho_{app,sol}(1-\varepsilon)$ (11)

where A is the reaction cross-section, and $\rho_{app,sol}$ is the apparent density of the solid. A similar model is applied to the MnAl₂O₄/MnAl₂O_{4- δ} system; however, in this case the model is simplified by the fact that the low value of δ [3] means that the gas flow rate and composition remain virtually unchanged along the height of the reactor. In addition, as confirmed by the results shown in Figure 2, the temperature changes are sufficiently low as to maintain the ratio between gas velocity and terminal velocity, appearing in Eq.(10), virtually constant. As a consequence, the average void fraction and overall bed height may be considered to be constant. In this case the reaction may be described as an irreversible reaction whose rate is given by a reaction-limited shrinking-core model, with a temperature-dependent kinetic constant [3]

$$X_{MnAl_2O_{4-\delta}} = 1 - (1 - t/\tau)^3 \quad ; \quad \tau = \frac{c_{MnAl_2O_{4-\delta}}R_g^0}{k_s c_{O_2}^g(\delta/2)} \quad ; \quad k_s = 5.33 \times 10^{-6} exp\left(-\frac{6.5[kJ/mol]}{RT}\right) \, [\text{mol/m}^2 \text{s}] \tag{12}$$

All symbols in Eq.(12) have the same meaning as in Eq. (7). The performance of the system was evaluated through the performance index, IP, defined according to Eq. (13). This index is significant in the case of FBRs because the gas flowrate is selected based on fluidization requirements, which pose stronger constraints compared to considerations on the rate of the chemical reactions; this entails that its value is quite high and remains virtually constant between inlet and outlet conditions.

$$IP = \frac{\int_0^t F_{out} c_{p,out} (T_{out} - T_{in}) dt'}{n_{CaO}^0 X(-\Delta H_r)}$$
(13)

4. Results

For both systems, the reactor modelled is a lab-scale fluidized bed, with a diameter of 3.5 cm loaded with 10 g of solid. Fig. 1 shows the results relative to a CaO carbonation reaction working at a pressure of 4 atm with an initial solid mass of 10 g, with a flow rate equal to five times the one required for minimum fluidization. The inlet feed temperature and initial solid temperature were both equal to 873 K. Fig. 1(a) refers to a feed gas containing 20% CO₂ and 80%

N₂, while panel (b) refers to a feed gas containing 5% CO₂. The black curves show solid conversion over time, while red curves show the average temperature. It should be noted that, given the assumption of perfectly mixed solid and the high rate of heat transfer between the two phases, the is uniform within the reactor. Results have been reported for conversions up to 40%, after which the reaction rate becomes limited by CO₂ diffusion through the solid ash layer and the process would therefore be slower than depicted in this simplified model. Panel (b) shows the gas temperature along the length of the reactor at different times. To explain the temperature profile, one must consider that, contrarily to what happens in fixed bed reactors, the reaction takes place simultaneously on all the solid. During the first seconds of the process, the heat released by the reaction causes an increase in the reactor temperature, up to a value that depends on the CO₂ in the feed. More precisely, the temperature reached in the reactor is such that the CO₂ concentration within the reactor approaches its equilibrium value at the temperature of the solid. Once these conditions have been achieved, the reaction proceeds at a rate that is almost constant, and the heat it releases is sufficient to maintain the equilibrium temperature achieved. From the comparison between panels (a) and (b), a decrease in the reaction rate when reducing the CO₂ concentration in the feed is clearly visible, along with a reduction in the maximum gas temperature. On the other hand, a slower reaction implies a longer duration of the discharge phase, which may lead a higher release of energy. This analysis highlights the importance of evaluating performance parameters to quantify the effect of both the duration of the discharge phase and the outlet gas temperature on the system performance. The height of the expanded bed was always equal to about 0.07 m, regardless of the actual temperature and gas composition in the reactor. This can be attributed to the high value of the difference between the solid and gas densities, which account for changes in the minimum fluidization and terminal velocities with gas composition, according to Eqs. (3) and (4), which make the term $(\rho_s-\rho_g)$ almost equal to ρ_g , under all the conditions considered here.

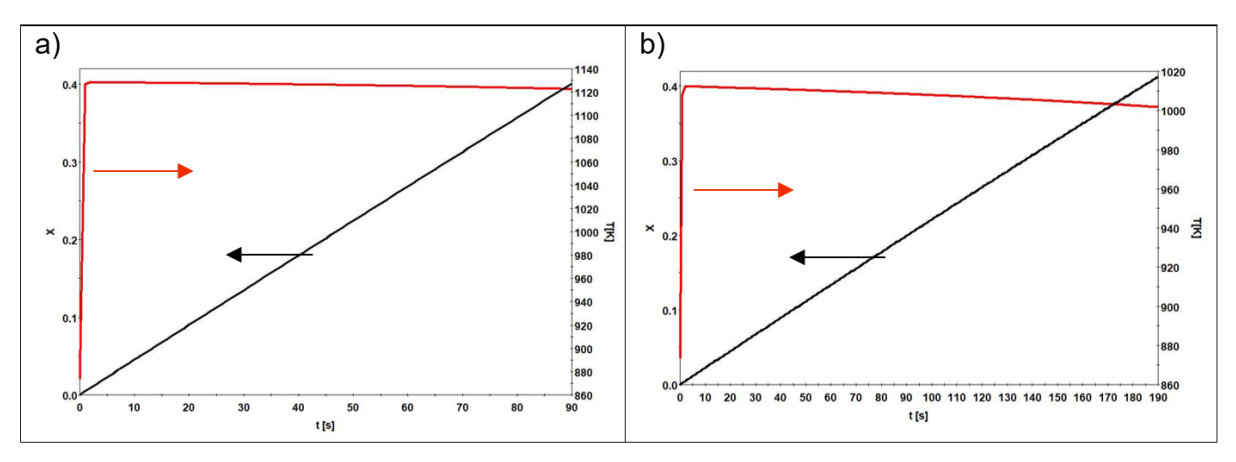


Figure 1. Solid conversion and average temperature over time with a feed gas containing 20% CO₂ (panel a) and 5% CO₂ (panel b). Other operating conditions are: inlet gas temperature equal to the initial solid temperature of 873 K, inlet gas velocity 5u_{mf}, pressure 4 atm.

Table 3 shows the performance index evaluated for two different CO_2 molar fractions in the inlet gas (0.20 and 0.05) at a pressure of 4 atm and gas velocity equal to 5 times the one required to achieve minimum fluidization conditions. The indexes have been evaluated for two cases, namely when the solid conversion is 30%, and at fixed time of 85 s. Interestingly, when the feed contains a lower amount of CO_2 , the efficiency obtained at fixed conversion is higher, because the duration of the discharge phase is longer, even though the outlet gas temperature is approximately 70 K lower than the one obtained with a higher CO_2 concentration. On the other hand, evaluating the performance for a fixed time rather than a fixed conversion, does not lead to significant differences in efficiency, but the overall amount of released energy increases significantly with the inlet CO_2 concentration. It is interesting to note that the results obtained here are perfectly in line with the more complex model developed in [8], in terms of reaction times, increase in gas temperature, and choice of gas velocity.

Table 3. Performance indicator for the CaO/CaCO₃ system for different CO₂ feed concentrations at 4 atm and $u = 5u_{mf}$

		$y_{CO_2} = 0.2$	$y_{CO_2} = 0.05$
X = 0.3			
	IP	0.695	0.717
	released energy [kJ]	6.66	6.84
	t required [s]	67	137
t = 85 s			
	IP	0.687	0.712
	released energy [kJ]	8.08	4.30
	X achieved	0.37	0.19

Figure 2 shows the main results obtained from the MnAl₂O₄/MnAl₂O_{4-δ} system, in which conversion was evaluated having considered a δ value of 0.04. In all the results shown, the feed to the reactor has been considered to have a flow rate equal to five times the one required to obtain minimum fluidization conditions. Gas temperatures (not shown for brevity) are uniform throughout the reactor and equal to that of the solid. The following observation may be made from an analysis of the results reported above: (i) a change in temperature does not have appreciable effects on the conversion time, because if, on the one hand, increasing temperature causes an increase on the kinetic constant, on the other hand it reduces the value of oxygen concentration in the gas; (ii) reducing pressure leads to an increase in the conversion time, because of the lower oxygen concentration in the gas, but the effect on outlet temperature is negligible. For a better understanding of the effect of operating conditions on the discharge phase, the performance indicator was evaluated for complete conversions (X = 1) and for a duration of the discharge step of 250 s. In the former case, the final time value was selected based on the moment in which full conversion was initially achieved, i.e. the sensible heat released after the completion of the reaction was not accounted for. The results are summarized in Table 4.

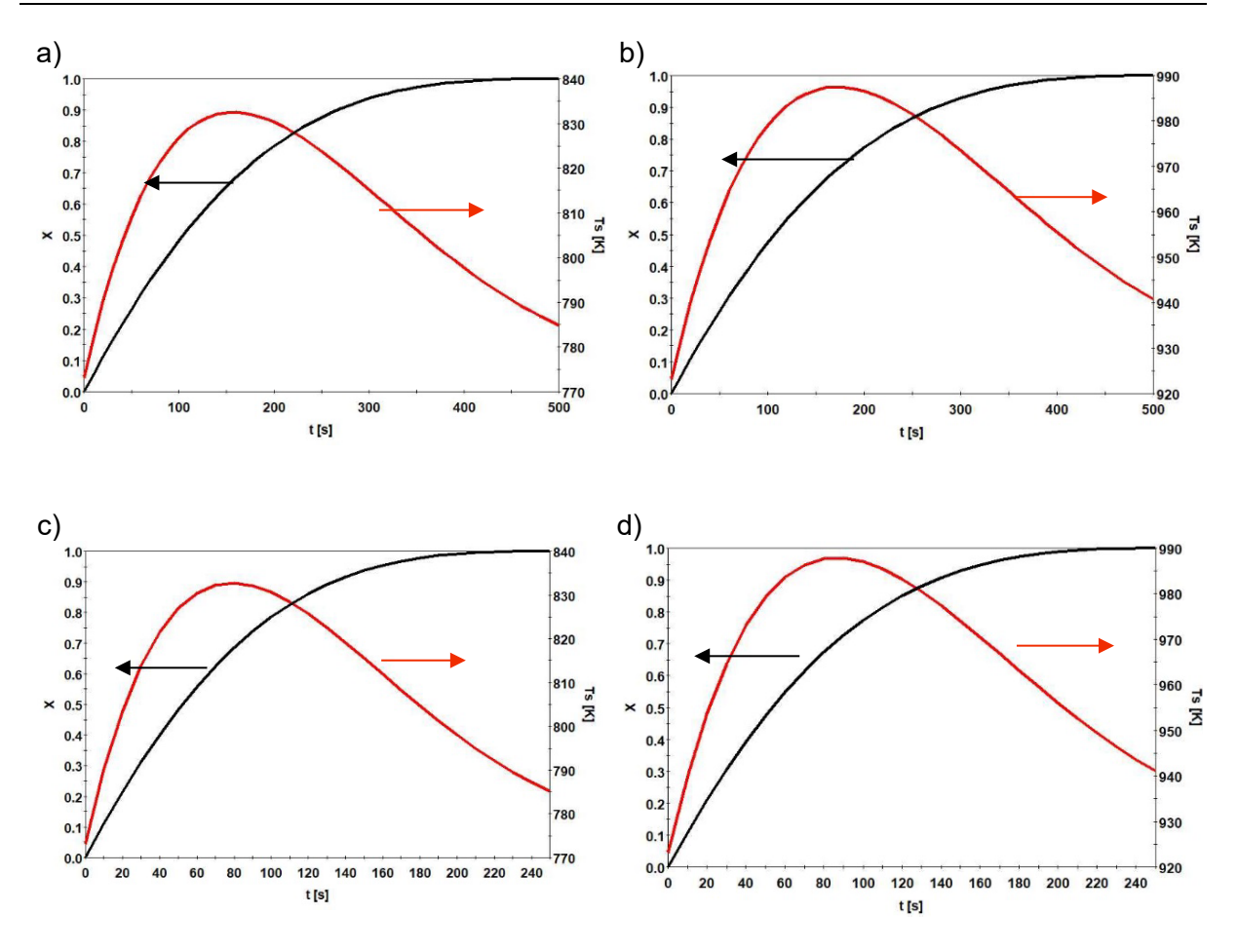


Figure 2. Solid temperature (black curve) and conversion (red curve) over time. In all panels the initial solid and inlet gas temperature are equal to each other. Results have been obtained under the following conditions: (a) 2 atm, 773 K, (b) 2 atm, 923 K, (c) 4 atm, 773 K, (d) 4 atm, 923 K

Table 4. Performance indicator for the MnAl₂O₄/MnAl₂O_{4- δ} system under different conditions. $u = 5u_{mf}$

		2 atm, 773 K	2 atm, 923 K	4 atm, 773 K	4 atm, 923 K
X = 1					
	IP	0.923	0.893	0.929	0.895
	released energy [kJ]	1.22	1.18	1.23	1.19
	t required [s]	500	500	250	250
t = 250 s					
	IP	0.645	0.585	0.925	0.888
	released energy [kJ]	0.75	0.67	1.22	1.18
	X	0.85	0.85	1	1

The values of the performance indicators show that, when working up to full conversion of the solid, the efficiency of the process depends weakly on both temperature and pressure. On the other hand, when considering a fixed time of the discharge process, pressure has a significant effect. This is linked to the fact that an increase in pressure from 2 to 4 atm causes a decrease in the complete conversion time, from 500 to 250 s.

5. Conclusions

The present work analyzed the performance of two distinct reactive systems during the discharge phase, which is well known to be the most critical phase of the storage process. The work showed that the CaO/CaCO₃ is, on average, characterized by lower efficiencies than that

based on the MnAl $_2$ O $_4$ /MnAl $_2$ O $_{4-\delta}$ couple, mainly because of the lower rate of reaction. On the other hand, because of the higher reaction enthalpy and lower molar mass of CaO, the former system has a higher overall storage capacity and has the additional advantage of an outlet gas temperature that is virtually constant over time, making coupling with a downhill power block simpler. The carbonation process is favored by higher CO $_2$ concentrations in the reacting gas, which increase the rate of reaction. The MnAl $_2$ O $_{4-\delta}$ oxidation is favored by higher pressures and lower initial temperatures.

Data availability statement

No additional data was used in the present work.

Author contributions

All authors contributed to: conceptualization, data curation, formal analysis, software, and writing.

Competing interests

The authors declare that they have no competing interests.

Funding

This work was funded by the Italian Ministry of Environment and Energy Security through Ricerca di Sistema Elettrico Nazionale (RdS), the «National Electricity System Research» programme. 2022-2024 triennial implementation plan. Integrated project 1.2: Energy Storage.

References

- [1] L.F. Marie, S. Landini, D. Bae, V. Francia, T.S. O'Donovan, "Advances in thermochemical energy storage and fluidised beds for domestic heat", J. Ener. Storage, vol. 53, pp. 105252, 2022, doi: https://doi.org/10.1016/j.est.2022.105242
- [2] S. Fegkas, F. Birkelbach, F. Winter, N. Freiberger, A. Werner, "Fluidized bed reactors of solid-gas thermochemical energy storage concepts modelling and process limitations", Energy, vol. 143, pp. 615-623, 2018.
- [3] T. Morabito, S. Sau, A.C. Tizzoni, A. Spadoni, M. Capocelli, N. Corsaro, C. D'Ottavi, S. Licoccia, T. Delise, "Chemical CSP storage system based on a manganes aluminium spinel," Sol. Ener., vol. 197, pp. 462-471, 2020, doi: https://doi.org/10.1016/j.solener.2020.01.007
- [4] S. Lo Conte, M.A. Murmura, F. Fratini, S. Cerbelli M. Lanchi, A. Spadoni, L. Turchetti, M.C. Annesini, "Calcium looping for thermochemical storage: assessment of intrinsic reaction rate and estimate of kinetic/transport parameters for synthetic CaO/Mayenite particles from TGA Data," Ind. & Eng. Chem. Res., vol.62, pp. 16523-16955, 2023, doi: https://doi.org/10.1021/acs.iecr.3c01820
- [5] D. Geldart, A.R. Abrahamsen. "Behaviour of gas-fluidized beds of fine powders. Part II. Voidage of the dense phase in bubbling beds". Powder Technology, vol. 26, pp. 47, 1980, doi: https://doi.org/10.1016/0032-5910(80)85006-6
- [6] A. Haider, O. Levenspiel. "Drag coefficient and terminal velocity of spherical and nonspherical particles". Powder Technology, vol. 58, pp. 63, 1989, doi: https://doi.org/10.1016/0032-5910(89)80008-7
- [7] M. Mamzehei, H. Rahmizadeh, "Experimental and numerical study of hydrodynamics with heat transfer in a gas-solid fluidized-bed reactor at different particle sizes", Ind. & Eng. Chem. Res., vol. 48, pp. 3177-3186, 2009, doi: https://doi.org/10.1021/ie801413q

[8] Guo, X., Zhou, W., Wei, J., "Numerical simulation of fluidized bed reactor for calcium looping energy release process in thermochemical storage: influence of key conditions", Ren. Energ., vol. 237, pp. 121532, 2024, doi: https://doi.org/10.1016/j.renene.2024.121532